Rapid Prototyping Human Interfaces Using Stretchable Strain Sensor

Yamaji, Tokiya

Nakamoto, Hiroyuki

Ootaka, Hideo

Hirata, Ichiro

Kobayashi, Futoshi

Research Article

Rapid Prototyping Human Interfaces Using Stretchable Strain Sensor

Tokiya Yamaji,[1] Hiroyuki Nakamoto,[1] Hideo Ootaka,[2] Ichiro Hirata,[3] and Futoshi Kobayashi[1]

[1]*Kobe University, 1-1 Rokkodaicho, Nada, Kobe 657-8501, Japan*
[2]*Bando Chemical Industries, 4-6-6 Minatojima Minamimachi, Chuo, Kobe 650-0047, Japan*
[3]*Hyogo Prefecture Institute of Technology, 3-1-12 Yukihiracho, Suma, Kobe 654-0037, Japan*

Correspondence should be addressed to Hiroyuki Nakamoto; nakamoto@panda.kobe-u.ac.jp

In the modern society with a variety of information electronic devices, human interfaces increase their importance in a boundary of a human and a device. In general, the human is required to get used to the device. Even if the device is designed as a universal device or a high-usability device, the device is not suitable for all users. The usability of the device depends on the individual user. Therefore, personalized and customized human interfaces are effective for the user. To create customized interfaces, we propose rapid prototyping human interfaces using stretchable strain sensors. The human interfaces comprise parts formed by a three-dimensional printer and the four strain sensors. The three-dimensional printer easily makes customized human interfaces. The outputs of the interface are calculated based on the sensor's lengths. Experiments evaluate three human interfaces: a sheet-shaped interface, a sliding lever interface, and a tilting lever interface. We confirm that the three human interfaces obtain input operations with a high accuracy.

1. Introduction

In the modern society with a variety of information electronic devices, human interfaces increase their importance in a boundary of a human and a device. In general, the human is required to get used to the device. Even if the device is designed as a universal device or a high-usability device, the device is not suitable for all users. The usability of the device depends on the individual user. Therefore, personalized and customized human interfaces are effective for the user. Recently, there are some papers with regard to personalized human interfaces. Kimura and Yamane used virtual product models to design human operational interfaces [1]. Ha et al. proposed a haptic prototyping system with a motor-actuated dial knob [2]. Their approaches aimed at design of common and high-usability interfaces. Yau et al. evaluated input devices for cursor-positioning tasks [3]. Turpin et al. evaluated computer input devices for people with disabilities and reported needs of customized interfaces [4]. Savage et al. proposed a system to assist designers creating human interface using a three-dimensional printer [5]. The customized interfaces improve working efficiency and help in using of devices for people with disability. To make the customized interfaces, technical foundations are being ready. One of the foundations is a three-dimensional printer (hereinafter referred to as "3D printer"). The 3D printer forms parts based on digital models and is effective for making parts of human interfaces. In addition, the cost of the 3D printer has gone down lately. Another of the technical foundations is a flexible sensor to obtain the motion of the parts.

Flexible and stretchable electronics have been developed. This technique applies elasticity to electronics. Developments advance from passive elements such as substrates, cables, and LEDs to functional elements such as actuators and sensors [6–10]. Application to various fields is considered using flexible and stretchable electronics, for example, production of an artificial muscle using electroactive macromolecule [11], development of artificial skin for robots using a flexible
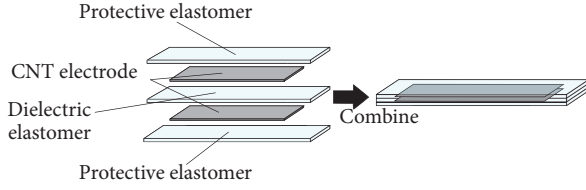
FIGURE 1: Structure of stretchable strain sensor.

sense of touch sensor [12], and measurement of the human knee's angle [13]. Flexible and stretchable sensors have been reported. Lipomi et al. proposed a strain sensor using the carbon nanotubes' electrodes [14]. In addition, Sato et al. reported various gesture detection using the sensing technology which enabled gesture input by measuring capacitance in a widespread frequency band [15]. We also proposed a stretchable strain sensor. The strain sensor is thin and lightweight and stretches up to 200% [16]. The combination of the 3D printer and the flexible sensor provides rapid prototyping human interfaces. The shape and size of the interfaces are easily changeable for users' needs. In this study, rapid prototyping human interfaces using a stretchable strain sensor are proposed. A 3D printer forms parts of interfaces. The motion of the constructed interfaces is measured by the strain sensors. The strain sensors are attached to the interfaces and measure the distances between the parts. The outputs of the interfaces are calculated based on the distances. Three kinds of interfaces are evaluated through laboratory experiments. It is confirmed that the interfaces using the 3D printer and the strain sensor are effective.

2. Stretchable Strain Sensor

2.1. Structure. The stretchable strain sensor has three thin sheets of elastomer and two stretchable electrodes. Figure 1 shows the structure of the stretchable strain sensor. The three elastic sheets sandwich the two electrode sheets. About the layers of the elastomer, the top and bottom layers have a role to protect electrodes. The middle layer has a role to be a dielectric layer. The elastomer is flexible and light weight. The thickness of the three-layer stretchable strain sensor is approximately 150 μm. The electrodes are made from carbon nanotubes [16]. The thickness of the electrode is less than 1 μm. Figure 2 shows the prototype of the stretchable strain sensor. The black part is the electrodes.

2.2. Measurement Principle. The stretchable strain sensor is assumed as a variable capacitor. Figure 3 shows the principle of the capacitance change of the strain sensor. The combination of the two electrodes and the sandwiched elastomer sheet builds a parallel plate type capacitor. The capacitance of the strain sensor depends on the area and thickness of the electrode's part (hereinafter referred to as "sensing part"). The capacitance of the strain sensor is given by

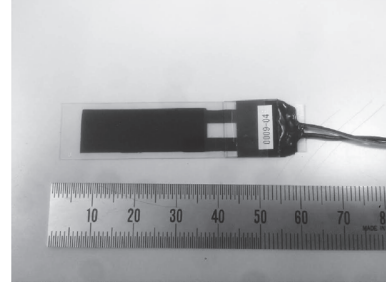$$C_0 = \varepsilon_r \varepsilon_0 \frac{hw}{d}, \tag{1}$$

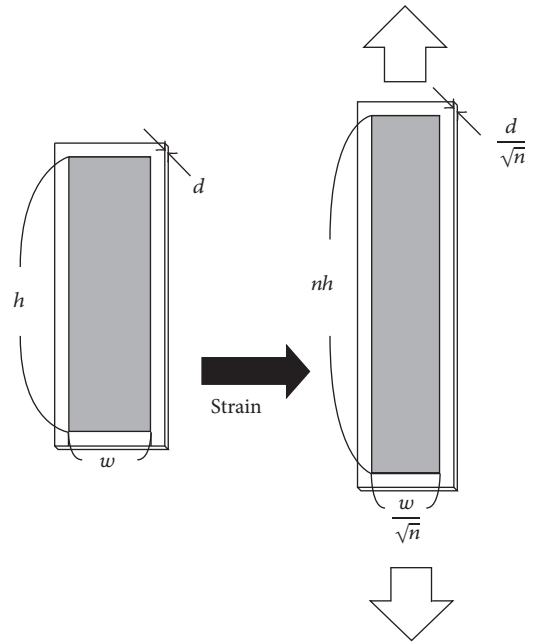FIGURE 2: Prototype of stretchable strain sensor.

FIGURE 3: Change in size of stretchable strain sensor.

where ε_r is the relative permittivity of the elastomer sheet, ε_0 is the permittivity in a vacuum, hw is the area of the sensing part, and d is the thickness of the sensing part. If Poisson's ratio of the sheet is approximately 0.5, the volume of the sensing part is assumed to be an almost constant. When the strain sensor is stretched to n-fold length in a single direction, the capacitance of the strain sensor is given by

$$C_n = \varepsilon_r \varepsilon_0 \frac{nhw/\sqrt{n}}{d/\sqrt{n}} = nC_0. \tag{2}$$

The length and the capacitance of the strain sensor are in a linear relationship. Therefore, the length of the strain sensor is determined based on the capacitance.

To confirm the relationship between the length and the capacitance of the strain sensor, a preliminary experiment was performed. Figure 4 shows the result of the relation between the capacitance of the strain sensor and the strain. The strain of natural length is 0%. Figure 4 shows that the length and the capacitance of the strain sensor are in a linear relationship. Table 1 shows the maximal errors of the target
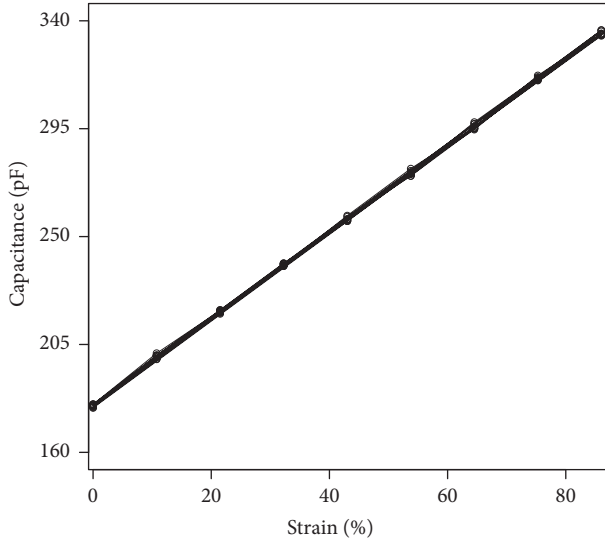
FIGURE 4: Relation between capacitance and strain.

TABLE 1: Maximal errors between target and estimate length.

	Maximal error [mm]
Sensor 0	0.51
Sensor 1	0.91
Sensor 2	0.48
Sensor 3	0.66

FIGURE 5: Structure of sheet-shaped interface.

FIGURE 6: Structure of sliding lever interface.

and estimate length. The maximal error was 0.91. It shows that the strain sensor has highly precise estimation.

3. Rapid Prototyping Human Interface

To make human interfaces, the stretchable strain sensors are applied to objects formed by a 3D printer. The 3D printer forms parts of the interfaces. The size of human interface depends on the size of human hands. The 3D printer is rapidly able to form an optimum human interface based on the size of the user's hand. Here, we make three types of interfaces: a sheet-shaped interface, a sliding lever interface, and a tilting lever interface. Both terminals of the strain sensor are attached to the parts of the interfaces. The strain sensor measures the distance between the parts as the length of itself. The output of the interface is determined based on the length of the strain sensor.

3.1. Sheet-Shaped Interface. The sheet-shaped interface comprises two frames formed by the 3D printer, one elastomer sheet, and the four strain sensors. Figure 5 illustrates the sheet-shaped interface. The frame is a 200 mm square and 5 mm in thickness. The elastomer sheet is 0.5 mm in thickness and is flexible and stretchable. The two frames sandwich the elastomer sheet and fix its periphery. The terminal of the strain sensor is attached to the frame, and the other terminal is attached to the center of the elastomer sheet. The four strain sensors are placed in the radial directions as shown in
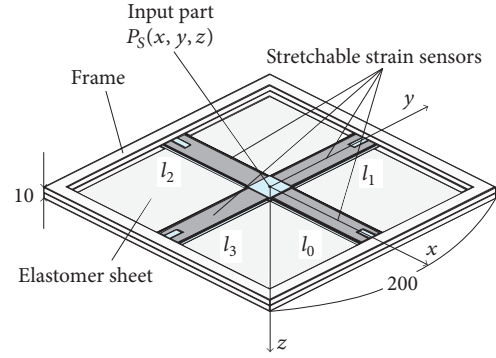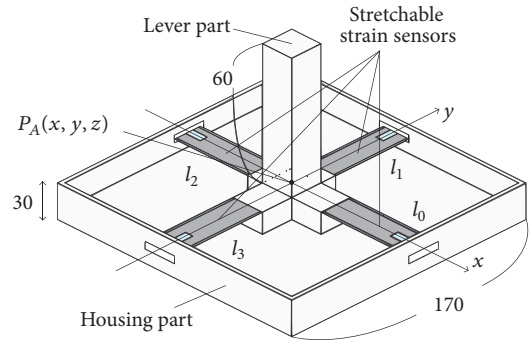
Figure 5. The center of the elastomer sheet is an input part. The four lengths of the strain sensors determine the three-dimensional displacement of the input part as the input of the interface. The displacement of the input part is geometrically given by

$$x = \sum_{i=0}^{3} k_{xi} l_i^2 + b_x, \tag{3}$$

$$y = \sum_{i=0}^{3} k_{yi} l_i^2 + b_y, \tag{4}$$

$$z = \sum_{i=0}^{3} k_{zi} l_i^2 + b_z, \tag{5}$$

where x, y, z are the three-dimensional displacement of the input part; the origin is placed at the center of the elastomer sheet. l_i is the length of the ith strain sensor. k_{xi}, k_{yi}, k_{zi} are coefficients for the square of the sensor's length and b_x, b_y, b_z are constants. The coefficients and the constants are determined based on the data set composed of the three-dimensional displacement of the input part and the lengths of the sensors by the least square method.

3.2. Sliding Lever Interface. The sliding lever interface comprises one lever part, one housing part, and the four strain sensors. Figure 6 shows the structure of the sliding lever interface. The lever and the housing parts are formed by the
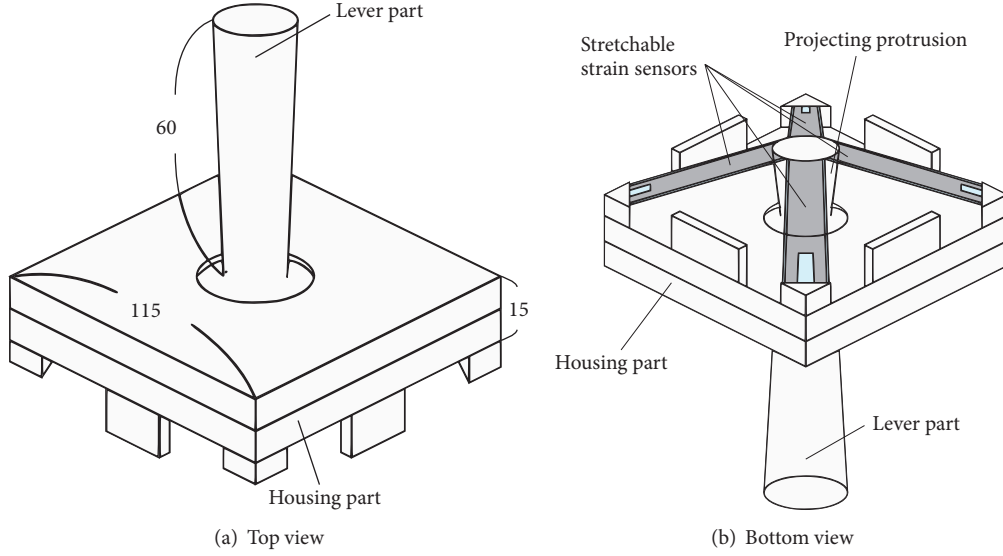
(a) Top view

(b) Bottom view

FIGURE 7: Structure of tilting lever interface.

3D printer. The housing part is 170 mm wide and 30 mm high. The height of lever part is 90 mm. The terminal of the strain sensor is attached to the wall of the housing and the other terminal is attached to the root of the lever. The lever smoothly slides in x-axis and y-axis directions. In the same manner with the sheet-shaped interface, x and y are determined by (3) and (4).

3.3. Tilting Lever Interface. The tilting lever interface comprises one lever part, two housing parts, and the four strain sensors. Figure 7 shows the structure of the tilting lever interface. The lever has a sphere shape at the lower part. The two housing parts sandwich the sphere. Therefore, the sphere rotates based on the tilting angle of the lever. The opposite end of the lever has a short projecting protrusion to attach the strain sensors. The other terminal of the strain sensor is fixed at the corner of the housing part. The coordinate axes for the interface are defined as shown in Figure 8. The origin of the coordinate axes is the center of the sphere in the lever. The two angles of the interface are defined as shown in Figure 9 and are estimated as follows. The three-dimensional position of the lever's bottom end is estimated based on the lengths of the strain sensor using (3)–(5). The relationship between the two angles, θ and ϕ, and the position of the bottom end is given by

$$\begin{pmatrix} x \\ y \\ z \end{pmatrix} = \begin{pmatrix} l_r \sin\theta \cos\phi \\ l_r \sin\theta \sin\phi \\ l_r \cos\theta \end{pmatrix}, \qquad (6)$$

where l_r denotes the length between the bottom end and the center of the sphere. θ and ϕ are given by

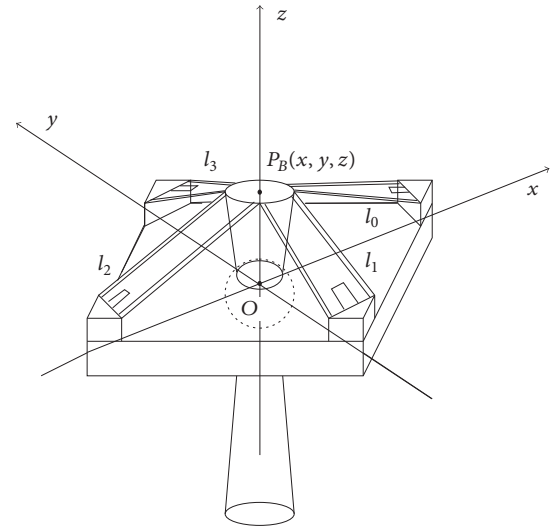$$\theta = \cos^{-1}\left(\frac{z}{\sqrt{x^2 + y^2 + z^2}} \right),$$

FIGURE 8: Coordinate axes of tilting lever interface.

$$\phi = \cos^{-1}\left(\frac{x}{\sqrt{x^2 + y^2}} \right).$$

(7)

4. Experiments

4.1. Experiment Flow. Experiments were performed to evaluate the accuracy of the interfaces. Figure 10 shows the experimental apparatus and the sliding lever interface. The experimental apparatus mainly comprises a motorized stage and a PC. The PC has an analog-digital conversion board and obtains the length of the strain sensor based on the measured capacitance. The motorized stage displaces the interface
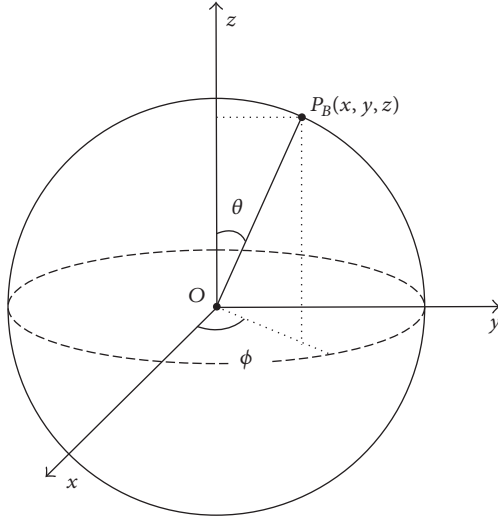
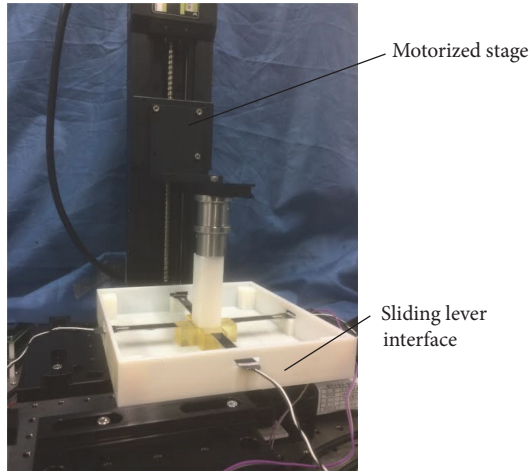FIGURE 9: Relation between coordinate axes and angles.

FIGURE 11: Prototype of sheet-shaped interface.

TABLE 2: Maximal errors between target and estimated displacements.

Axis	Maximal error [mm]
x ($z = 11$)	1.32
y ($z = 11$)	0.75
x ($z = 16.5$)	0.67
y ($z = 16.5$)	0.61
x ($z = 22$)	1.21
y ($z = 22$)	1.45
z	3.77

FIGURE 10: Experimental apparatus for sliding lever interface.

through the stage in x-axis, y-axis, and z-axis directions. The precision of the displacement is 0.01 mm. The experimental flow is as follows. First, the data sets for calibration are obtained using the motorized stage. The coefficients and constants expressed in (3)–(5) are determined based on the data sets. Second, the motorized stage displaces the interface again. The PC estimates the outputs of the interface. The displacements of the motorized stage and the outputs of the interface are compared.

4.2. Sheet-Shaped Interface. Figure 11 shows the prototype of the sheet-shaped interface. Although the natural length of the strain sensor is 46.5 mm, each strain sensor was attached to the elastomer sheet while being stretched to 62 mm. The displacements were −6.0, −3.0, 0, 3.0, and 6.0 mm in x-axis and y-axis directions and were 11.0, 16.5, and 22.0 mm in z-axis direction. Therefore, the number of the displacements' combinations was 75. Figures 12–14 show the relationships between target and estimated displacements in x-axis and
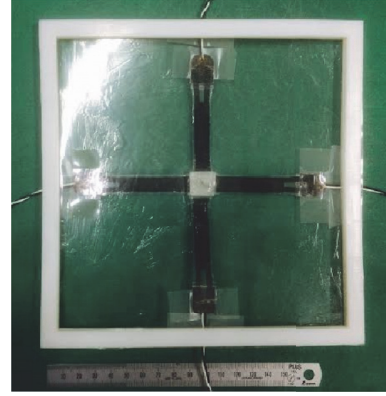
y-axis. In this paper, including graphs, target means true value measured by a motorized machine. Figure 15 shows the results in z-axis. In addition, Table 2 shows maximal errors in each axis.

4.3. Sliding Lever Interface. Figure 16 shows the prototype of the sliding lever interface. The strain sensors were stretched to 77 mm and were attached to the root of the lever and the side of the housing part. After the calibration was performed, the lever was slid −12.0, −8.0, −4.0, 0, 4.0, 8.0, and 12.0 mm in x-axis and y-axis directions. Therefore, the number of the displacements' combinations was 49. Figures 17(a) and 17(b) show the relationships between target and estimated displacements in x-axis and y-axis. Table 3 shows maximal errors in each axis.

4.4. Tilting Lever Interface. Figure 18 shows the prototype of the tilting lever interface. The strain sensors were stretched to 70 mm and were attached to the bottom side of the lever part as shown in Figure 7(b). The lever was tilted in the experiment. The angles of θ were 10°, 20°, and 26°. The angles of ϕ were 0°, 45°, 90°, 135°, and 180°. The number of the angles' combinations was 15. Figure 19 shows the relationships between target and estimated angles of θ and ϕ. Table 4 shows maximal errors of each angle.
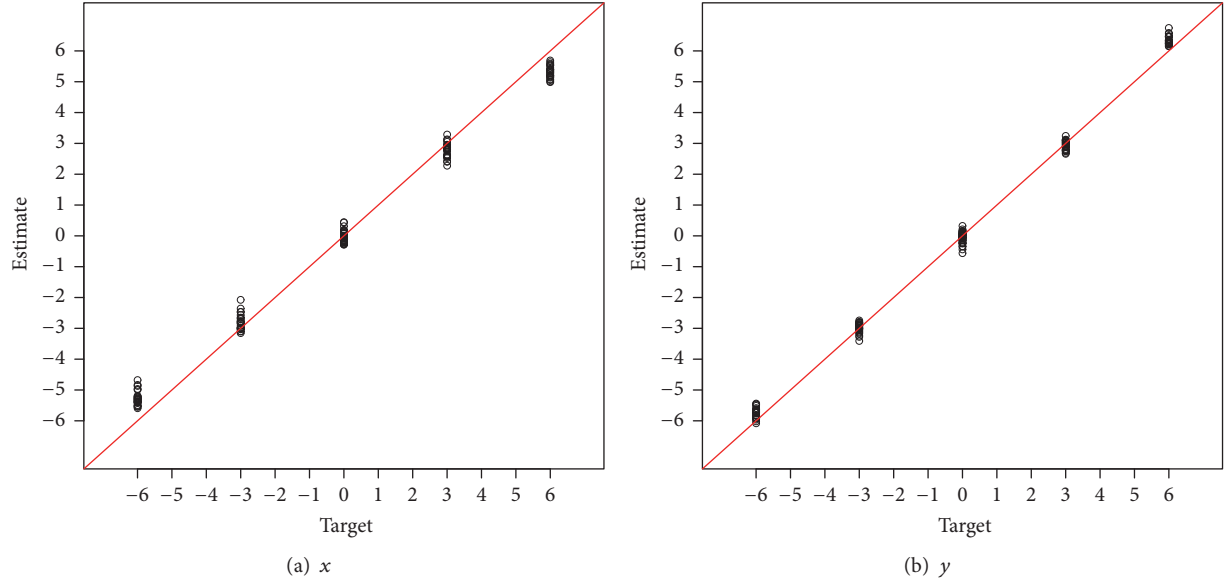
(a) x

(b) y

FIGURE 12: Relation between target and estimated displacements under the condition of $z = 11$.
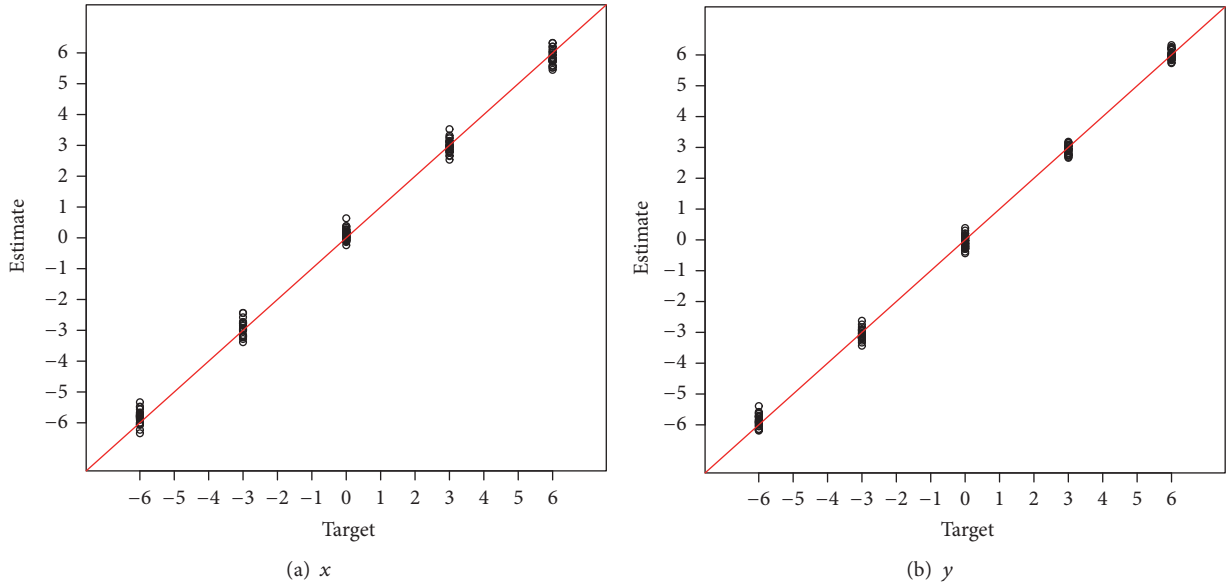

(a) x

(b) y

FIGURE 13: Relation between target and estimated displacements under the condition of $z = 16.5$.

TABLE 3: Maximal errors between target and estimated displacements.

Axis	Maximal error [mm]
x	0.73
y	1.00

TABLE 4: Maximal errors between target and estimate.

Angle	Maximal error [°]
θ	2.82
ϕ	10.88

5. Discussion

The proposed interface has the sheet-shaped and the lever-shaped structures. They are fundamental structure for interfaces and have the ability to enhance personalized interfaces

by changing the size and shape of the parts. Here, we discuss the accuracy of the fundamental interfaces.

The sheet-shaped interface had small maximal errors in x-axis and y-axis in Table 2. Because the strain sensor had a measurement error within 5%, the maximal errors in x-axis and y-axis were conceivable. On the other hand, the

(a) x

(b) y

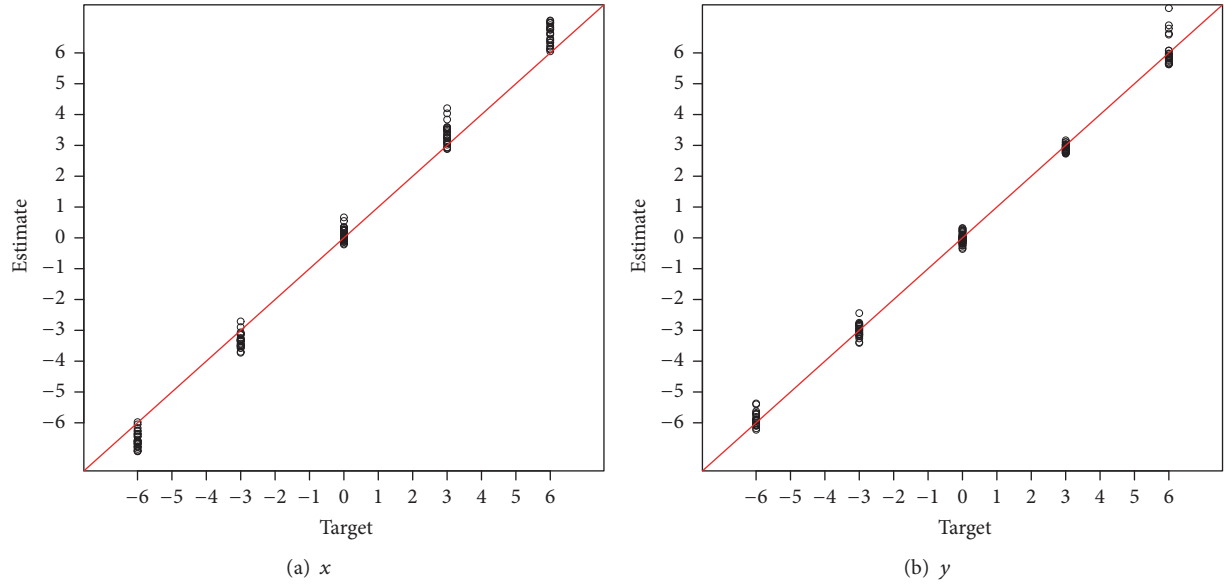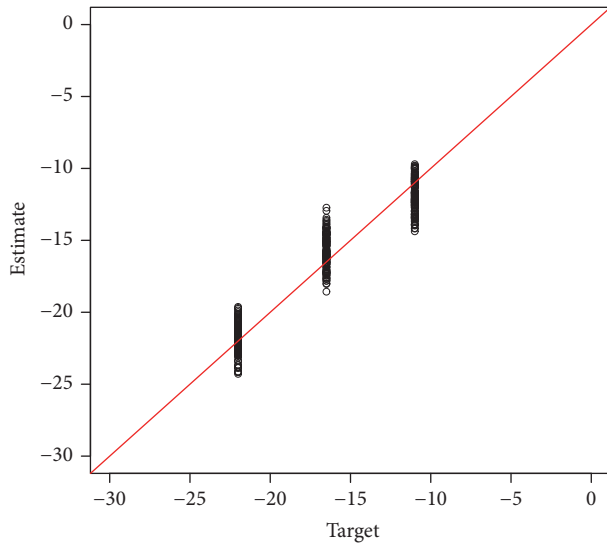FIGURE 14: Relation between target and estimated displacements under the condition of $z = 22$.

FIGURE 15: Relation between target and estimated displacements in z-axis.

FIGURE 16: Prototype of sliding lever interface.

maximal error in z-axis was 3.77 mm. Although the error of z-axis is relatively large compared to the errors of x-axis and y-axis, the range of z-axis displacement is also large. We consider that a small range improves the error. The maximal errors of the sliding lever interface were as much as those of the sheet-shaped interface. The sliding lever interface used the four strain sensors for the estimate of the two-axis displacement. The number of the strain sensors was redundant and increased the accuracy of the estimate. The tilting lever interface had the large difference between the errors of θ and ϕ. The main reason of the difference was the difference of the angle range. In Figure 19(b), the errors were almost constant in the whole range.
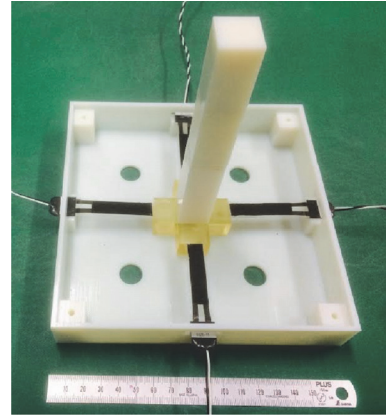
The results of the three interfaces showed that the errors had no bias. Actually, the outputs of the interfaces against continuous input were smooth. This characteristic is effective for interface devices. The errors of the outputs mainly depended on the measurement errors of the strain sensor, which were shown in Table 1. The rates of their errors to the output ranges were almost constant at 10%. To reduce the measurement errors, it is necessary to improve the composition and the circuit of the strain sensor.

6. Conclusion

The rapid prototyping human interfaces using the stretchable strain sensor were proposed. The parts of the interfaces were formed by the 3D printer, and it was easy to change their size and shape. The combinations of the parts and the four strain sensors produced the three interfaces: the sheet-shaped interface, the sliding lever interface, and the tilting lever
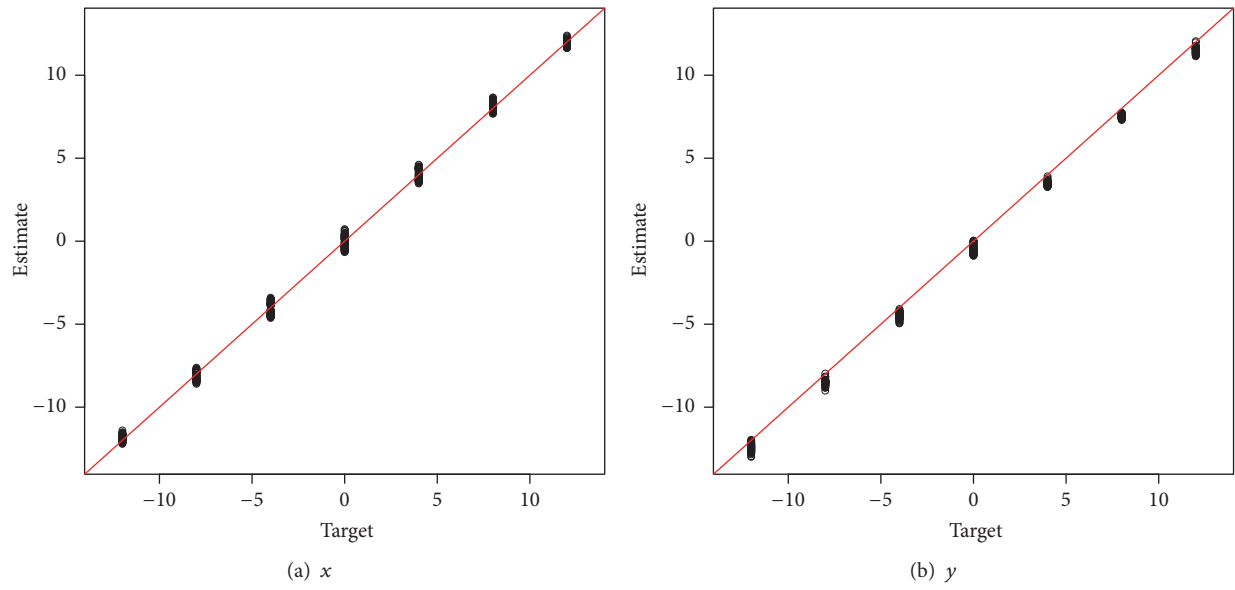
(a) x

(b) y

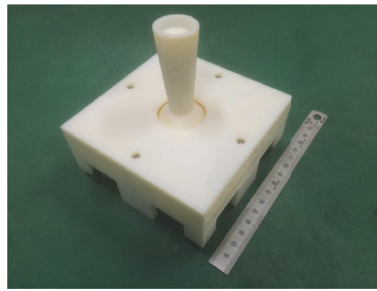Figure 17: Relation between target and estimated displacements of the lever sliding lever interface.

Figure 18: Prototype of tilting lever interface.
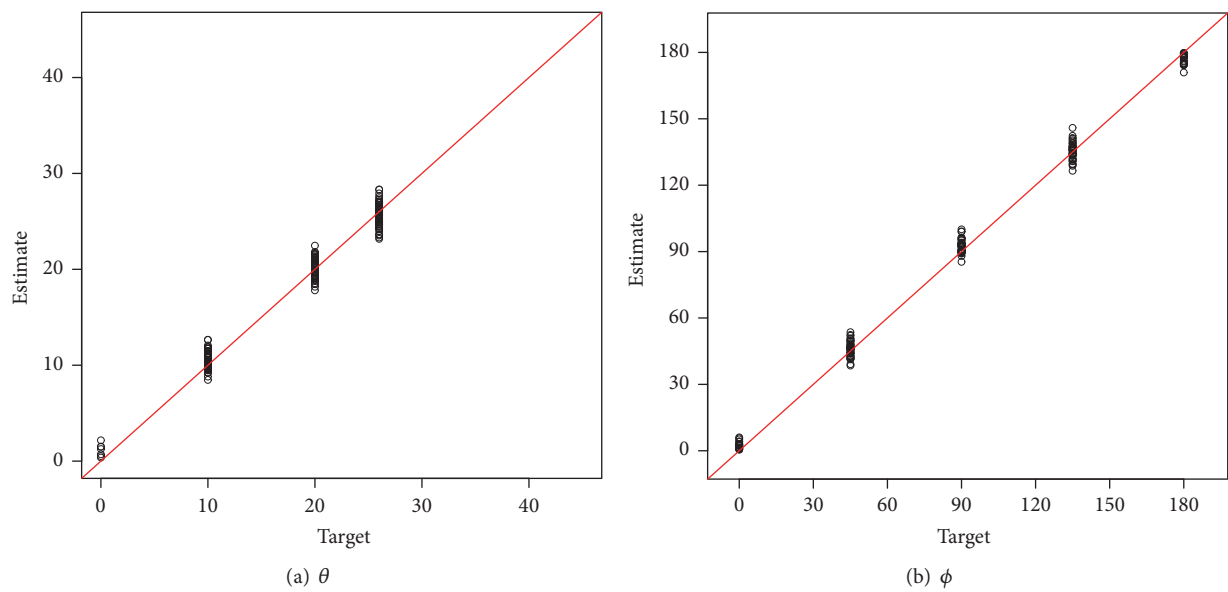

(a) θ

(b) ϕ

Figure 19: Relation between target and estimate of tilting lever interface.

interface. The rates of their errors to the output ranges were almost constant. The characteristic without bias is suitable for human interface devices. To improve the resolution of the interface's output, it is necessary to optimize the composition and the circuit of the strain sensor. In addition, the strain sensor is being applied to other interfaces, such as wearable interfaces.

Competing Interests

The authors declare that there are no competing interests regarding the publication of this paper.

Acknowledgments

References

[1] F. Kimura and N. Yamane, "Haptic environment for designing human interface of virtual mechanical products," *CIRP Annals—Manufacturing Technology*, vol. 55, no. 1, pp. 127–130, 2006.

[2] S. Ha, L. Kim, S. Park, C. Jun, and H. Rho, "Virtual prototyping enhanced by a haptic interface," *CIRP Annals—Manufacturing Technology*, vol. 58, no. 1, pp. 135–138, 2009.

[3] Y. J. Yau, S. L. Hwang, and C. J. Chao, "Effects of input device and motion type on a cursor-positioning task," Perceptual and Motor Skills, pp. 7690, 2008.

[4] G. Turpin, J. Armstrong, P. Frost, B. Fine, C. D. Ward, and L. L. Pinnington, "Evaluation of alternative computer input devices used by people with disabilities," *Journal of Medical Engineering and Technology*, vol. 29, no. 3, pp. 119–129, 2005.

[5] V. Savage, C. Chang, and B. Hartmann, "Sauron: embedded single-camera sensing of printed physical user interfaces," in *Proceedings of the 26th Annual ACM Symposium on User Interface Software and Technology (UIST '13)*, pp. 447–456, St Andrews, UK, October 2013.

[6] D.-Y. Khang, H. Jiang, Y. Huang, and J. A. Rogers, "A stretchable form of single-crystal silicon for high-performance electronics on rubber substrates," *Science*, vol. 311, no. 5758, pp. 208–212, 2006.

[7] D.-H. Kim and J. A. Rogers, "Stretchable electronics: materials strategies and devices," *Advanced Materials*, vol. 20, no. 24, pp. 4887–4892, 2008.

[8] T. Sekitani, H. Nakajima, H. Maeda et al., "Stretchable active-matrix organic light-emitting diode display using printable elastic conductors," *Nature Materials*, vol. 8, no. 6, pp. 494–499, 2009.

[9] R. Pelrine, R. Kornbluh, Q. Pei, and J. Joseph, "High-speed electrically actuated elastomers with strain greater than 100%," *Science*, vol. 287, no. 5454, pp. 836–839, 2000.

[10] C. Stampfer, T. Helbling, D. Obergfell et al., "Fabrication of single-walled carbon-nanotube-based pressure sensors," *Nano Letters*, vol. 6, no. 2, pp. 233–237, 2006.

[11] F. Carpi, R. Kornbluh, P. Sommer-Larsen, and G. Alici, "Electroactive polymer actuators as artificial muscles: are they ready for bioinspired applications?" *Bioinspiration and Biomimetics*, vol. 6, no. 4, Article ID 045006, 2011.

[12] Q. Gao, H. Meguro, S. Okamoto, and M. Kimura, "Flexible tactile sensor using the reversible deformation of poly(3-hexylthiophene) nanofiber assemblies," *Langmuir*, vol. 28, no. 51, pp. 17593–17596, 2012.

[13] B. J. Munro, T. E. Campbell, G. G. Wallace, and J. R. Steele, "The intelligent knee sleeve: a wearable biofeedback device," *Sensors and Actuators, B: Chemical*, vol. 131, no. 2, pp. 541–547, 2008.

[14] D. J. Lipomi, M. Vosgueritchian, B. C.-K. Tee et al., "Skin-like pressure and strain sensors based on transparent elastic films of carbon nanotubes," *Nature Nanotechnology*, vol. 6, no. 12, pp. 788–792, 2011.

[15] M. Sato, I. Poupyrev, and C. Harrison, "Touché: enhancing touch interaction on humans, screens, liquids, and everyday objects," in *Proceedings of the SIGCHI Conference on Human Factors in Computing Systems (CHI '12)*, pp. 483–492, Austin, Tex, USA, May 2012.

[16] H. Nakamoto, H. Ootaka, M. Tada, I. Hirata, F. Kobayashi, and F. Kojima, "Stretchable strain sensor based on areal change of carbon nanotube electrode," *IEEE Sensors Journal*, vol. 15, no. 4, pp. 2212–2218, 2015.